Crystallization Processes in Poly(Ethylene Terephthalate) as Modified by Polymer Additives and Fiber Reinforcement

VERONIKA E. REINSCH and LUDWIG REBENFELD*

TRI/Princeton, and Department of Chemical Engineering, Princeton University, P.O. Box 625, Princeton, New Jersey 08542

SYNOPSIS

The effect of fiber reinforcement on the crystallization kinetics of poly(ethylene terephthalate), or PET, was investigated using differential scanning calorimetry. The objective of the study was to determine how the effects of fiber reinforcement on PET crystallization are modified by the presence of polymer nucleating and plasticizing additives. Unidirectional fiber composites were prepared using aramid and glass fibers in PET. The rate of crystallization of PET, as reflected by crystallization half-time, is seen to depend on reinforcing fiber type, crystallization temperature, and presence of nucleant or plasticizer. However, degree of crystallinity of PET is largely unaffected by the presence of additives and reinforcing fibers. Crystallization kinetics are analyzed using the Avrami model for PET volume crystallized as a function of time. Avrami plots for PET and fiber-reinforced PET exhibit two linear regions, possibly corresponding to primary and secondary crystallization. The crystalline morphology of fiber-reinforced PET was also studied using polarized light microscopy. Results concerning nucleation density and growth morphology are used in explaining differences seen in crystallization kinetics in fiber-reinforced systems. © 1994 John Wiley & Sons, Inc.

INTRODUCTION

Crystallization of poly(ethylene terephthalate), or PET, has been the subject of extensive study. Thermally induced crystallization in PET develops a spherulitic structure, with spherulitic radii typically varying from 6 to 50 μm, depending on crystallization conditions and the polymer sample.[1,2] Thermally crystallized PET viewed by polarized light transmission microscopy usually reveals the typical Maltese cross type of extinction pattern, or a form in which zigzag patterns replace the arms of the Maltese cross.[3,4] Studies of PET crystallization using depolarized light intensity and small-angle light scattering indicate that significant crystallization also takes place outside of the spherulitic structures.[5] The kinetics of PET crystallization depend on crystallization temperature, sample molecular weight, and catalyst residue.[1,6-8] Diethylene glycol, produced in a side reaction during industrial synthesis of PET, has also been found to affect crystallization kinetics.[9-12]

In order to accommodate typical industrial injection molding processes, additives (most often nucleating agents) are introduced to increase the rate of PET crystallization. Inorganic compounds such as talc have been found to enhance crystallization by dense heterogeneous nucleation on the surface of additive particles.[13] Similarly, enhancement of crystallization rate has been observed in PET containing kaolin or titanium dioxide, for nucleant particle sizes under 5 μm.[13] Large kaolin and TiO_2 particles (particle diameters from 50 to 70 μm) have been observed to depress the crystallization rate of PET.[14] Metal hydroxides capable of releasing water nucleate PET, while metal hydroxides incapable of releasing water do not.[15] Localized severe hydrolysis of PET or supercooling in the vicinity of released water have been proposed as possible mechanisms for enhanced PET nucleation.[15] Certain sodium containing compounds have been found to nucleate crystallization, presumably by chain scission to create PET chains with ionic end groups that form ag-

Journal of Applied Polymer Science, Vol. 52, 649–662 (1994)
 CCC 0021-8995/94/050649-14

gregates that serve as nucleation sites for crystal growth.[16,17] Kim and Kim[18] note that the vigorous mixing used to introduce additives, as well as the additives themselves, affects PET crystallization through a memory effect of shear history.

The effect of reinforcing fibers on the crystallization of thermoplastic polymer matrices in which they are imbedded has been studied for a variety of composite systems (e.g., Refs. 19–22). For PET reinforced with continuous glass fibers (fiber diameter = 14 μm), an enhancement of the rate of PET crystallization from the glassy state has been observed.[23] For PET filled with short glass fibers (length = 1 mm, diameter = 90 μm), a depression in rate of crystallization from the melt has been observed.[14] We have previously studied the effect of glass and Kevlar 49 aramid fibers on the isothermal crystallization of PET from the melt using differential scanning calorimetry (DSC) and polarized light microscopy.[24] Fiber reinforcement was found to enhance the rate of crystallization, as quantified by crystallization half-time, with Kevlar fibers producing a greater increase in crystallization rate than glass fibers. This effect was attributed to sites for crystal nucleation located on the fiber surface. In the case of Kevlar fibers, polarized light microscopy of model thin film composites showed that nucleation sites are so densely located on the fiber surface that polymer crystals are constrained to grow linearly outward from the fiber surface, producing a crystal morphology near the fiber surface distinctly different from that in the bulk of the polymer. Such a region is often termed a transcrystalline region.

Fiber surface treatments, or sizings, were also found to affect polymer properties. In composites prepared with sized Kevlar fibers, a depression in the glass transition temperature, or T_g, of PET was observed.[24] Similar effects have been observed in polyphenylene sulfide composites.[25] In both studies, the depression in T_g was ascribed to the diffusion of sizing into the polymer matrix and plasticization by a component in the sizing formulation. Thus, in past studies, the introduction of fibers in a polymer matrix has been observed to affect (depending on the type of reinforcing fiber as well as the matrix) both the rate of crystallization, presumably by enhanced crystal nucleation on the fiber surface, and the glass transition temperature, presumably through plasticization caused by a component in the sizing.

In the current study, we are interested in the interaction between the effects of fibers and typical commercial polymer additives on PET crystallization. Unidirectional, continuous fiber composites were prepared using Kevlar and glass fibers (both with and without commercial fiber surface treatments). The matrix polymers used were PET, PET with added nucleating agent, and PET with added plasticizing agent. Crystallization kinetics were studied by DSC in isothermal crystallizations from the melt, and glass transition temperatures were measured in dynamic DSC scans. These results were complemented by studies of polymer morphology with polarized light microscopy on model thin films. In this study, we attempt to reveal more about the mechanisms regarding nucleation and plasticization effects by fibers and fiber sizings on PET crystallization.

EXPERIMENTAL

The three samples of polymer, supplied by Hoechst Celanese in pellet form for use in this study, were PET, the same PET with commercial nucleating agent added, and the same PET with commercial plasticizing agent added. The pellets were molded into films on a hot press for 1 min at 275°C and 1000 psi, between two sheets of Teflon-coated glass release fabric (TM 7038, supplied by Taconic Plastics). The fiber composites used in this study were prepared in our laboratory using compression molding. Between 5 and 20 fiber tows were "sandwiched" between two pieces of prepared PET film and two pieces of release fabric in an aluminum mold with well dimensions 1.6 × 2.9 cm. The mold was then held at 275°C and 150 psi for 10 min on a hot press. Employing this technique, the following composites were prepared with each of the three PET matrix films: 54 wt % unsized Kevlar, 48 wt % sized Kevlar, 55 wt % water-sized glass, and 58 wt % PET-compatible-sized glass fiber. These fiber loadings, although they vary in terms of weight percent, were chosen to provide the same overall interfacial contact area (i.e., differences in fiber diameter and density are accounted for, in order to produce the same fiber surface area per gram polymer in each composite). Twice-molded film was then prepared for the unreinforced matrix polymers, by inserting two pieces of film (no fibers) into an aluminum mold and compression molding as described above. The purpose of this double molding was to ensure that the unreinforced PET experienced the same thermal history and exposure to release substances as the PET in the composites. All samples were dried for 15 h at 100°C in a vacuum oven.

Three complete cross-sectional specimens of each composite (weighing between 10 and 15 mg), and three samples of each of the twice-molded unrein-

forced films (roughly 5 mg) were then prepared for use in DSC. Initially, the sample was scanned from 25 to 290°C at 10°C/min, and data of heat flow as a function of temperature were collected. The sample was held at 290°C for 3 min to achieve complete melting, and then quenched at a rate of 320°C/min to the isothermal crystallization temperature of interest, where data of heat flow as a function of time were collected. When heat flow no longer changed with time, the sample was cooled to 15°C below the crystallization temperature, then scanned to 290°C at 10°C/min while data of heat flow as a function of temperature were collected for the fusion process. The sample was again held at 290°C for 3 min, quenched to the next crystallization temperature, and data were collected as described above. The procedure was repeated until the last crystallization temperature was reached.

The effects of reinforcing fibers and polymer additives on PET morphology were also investigated using polarized light microscopy. Model thin film specimens were prepared by placing 4–5 small pieces of PET film, totaling approximately 3 mg, on a glass microscopy coverslip. Roughly 10 single filaments were then placed singly over the film. The assembly was placed on the bottom plate of the hot press maintained at 320°C. When the PET was observed to melt, another coverslip was placed over the original and pressure was exerted. The melting temperature of 320°C was needed to reduce viscosity in order to produce very thin films suitable for light microscopy. When a sufficiently thin film was achieved, the second coverslip was removed and discarded, while the PET film was crystallized from the melt for 1 min substantially above T_g, and then rapidly quenched to room temperature in order to "freeze" the crystallization at an early stage. This sample preparation procedure was found to better elucidate the interaction between fibers and matrix, particularly in the early stages of crystalline growth, than a procedure that more closely mimics the treatment of samples during DSC experiments.

RESULTS AND DISCUSSION

Morphology

Optical micrographs of fibers embedded in PET show a range of morphological effects. PET and plasticized PET both display a vigorously nucleated region of linear growth, or transcrystallinity, on the surface of sized and unsized Kevlar fibers. Far from the fiber surface, the bulk morphology is spherulitic with typical Maltese cross extinction patterns characteristic of PET crystallization below 180°C.[3] A sample micrograph is shown in Figure 1. Glass fibers, both water-sized and PET-compatible-sized, in the same matrices display a less pronounced nucleating ability, as, for example, in Figure 2. The bulk morphology is the same as that shown in Figure 1. The morphology of nucleated PET is very different from that of the other matrices. The additive produces crystals nucleated so densely that the observed

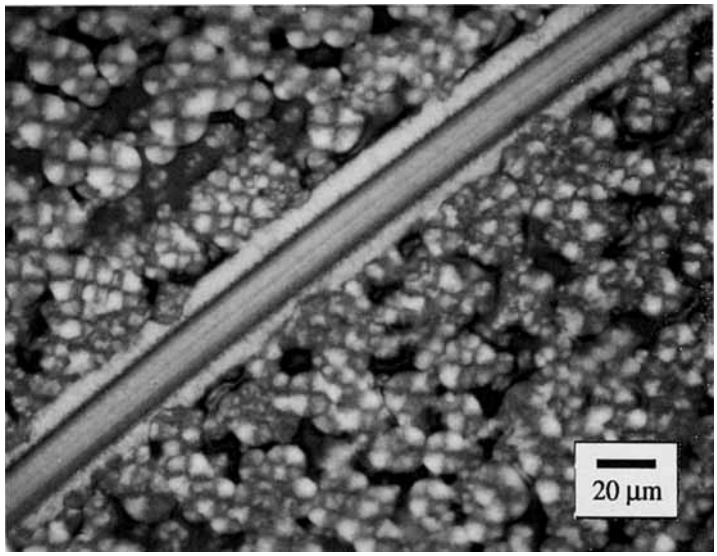

Figure 1 Polarized light micrograph of sample thin-film specimen of unsized Kevlar fiber in PET matrix. 360× magnification.

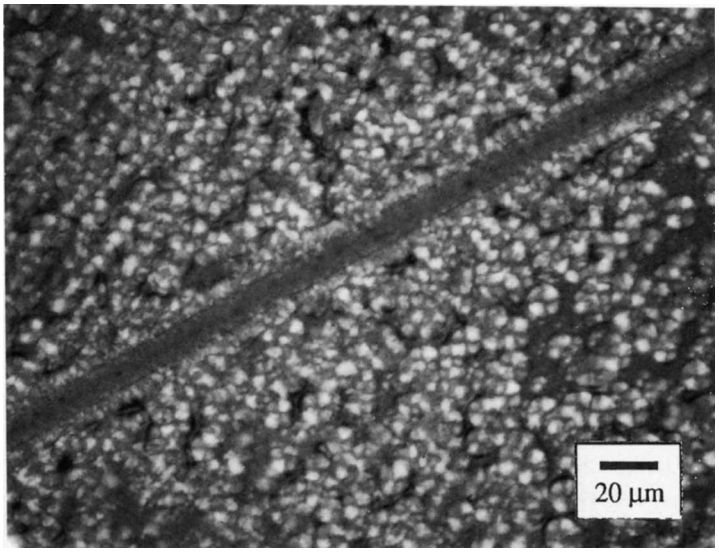

Figure 2 Polarized light micrograph of sample thin-film specimen of water-sized glass fiber in plasticized PET matrix. 360× magnification.

crystalline texture is fine, granular, and without recognizable spherulites of significant size. Fibers have no effect on the morphology of the nucleated PET sample; nucleation in the bulk is so dense that the fibers appear inert (Fig. 3).

Crystallization Rate

The relative crystallinity at time t, $C(t)$, is obtained from the DSC crystallization isotherm as the area under the peak at time t divided by the total area under the peak:

$$C(t) = \frac{\int_0^t (\Delta H/dt)\, dt}{\int_0^\infty (\Delta H/dt)\, dt} \qquad (1)$$

Plots of relative crystallinity as a function of time

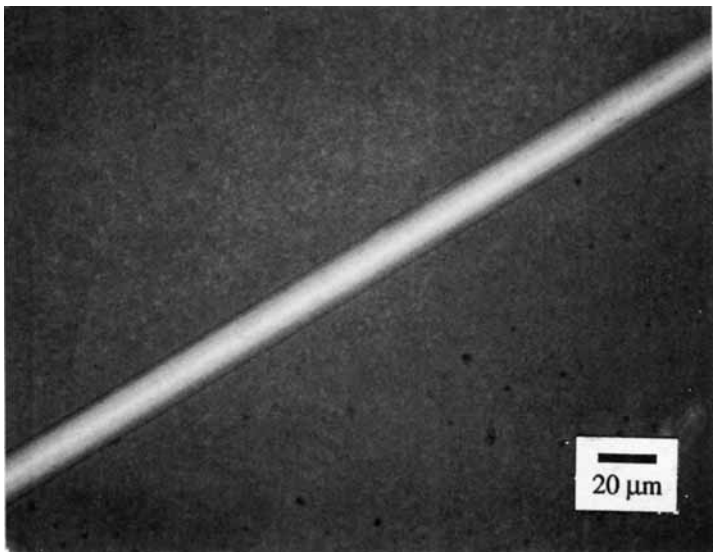

Figure 3 Polarized light micrograph of sample thin-film specimen of unsized Kevlar fiber in nucleated PET matrix. 360× magnification.

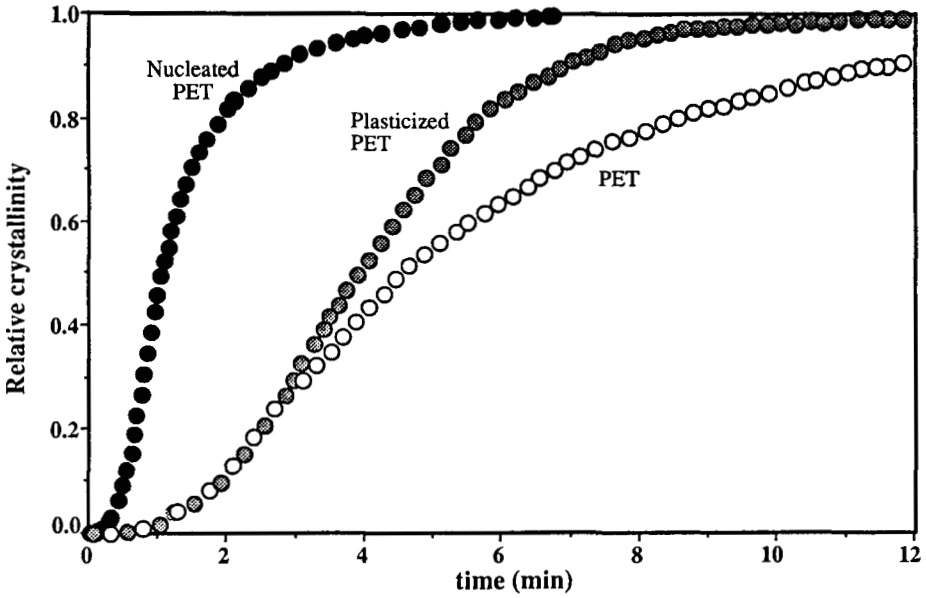

Figure 4 Relative crystallinity as a function of time for unreinforced PET films at a crystallization temperature of 230°C. Curves reflect the average of three data sets collected per sample.

show the development of crystallinity in the polymer over time. Sample relative crystallinity plots are shown in Figure 4 for the twice-molded films of PET, PET with nucleant, and PET with plasticizer at a crystallization temperature of 230°C. The marked effect of nucleating agent is apparent. The addition of the nucleating agent strongly enhances crystallinity development in the early stages of crystallization, which are dominated by nucleation events. In contrast, the plasticizer enhances the development of crystallinity only in the later stages of growth. This effect reflects the greater chain mobility produced by the plasticizing additive, thereby reducing chain entanglements, which are common in the later stages of growth.

The kinetics of crystallization can be quantified by a crystallization rate, which can be taken to be the inverse of the crystallization half-time. The

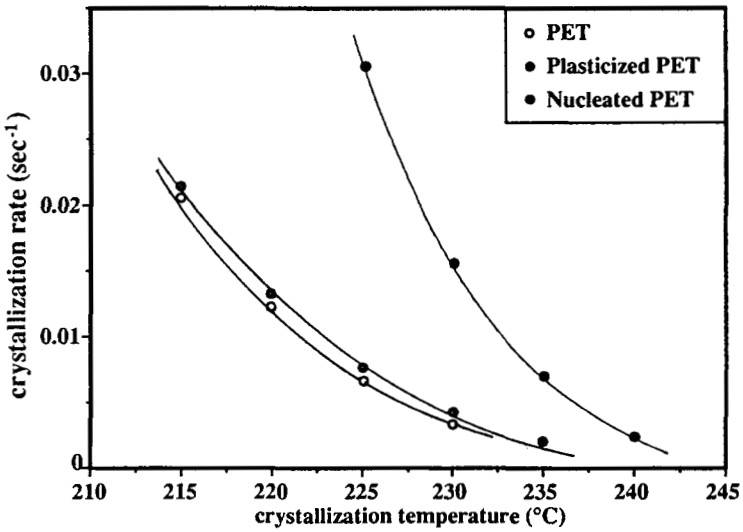

Figure 5 Crystallization rate ($1/t_{1/2}$) as a function of crystallization temperature for unreinforced PET films.

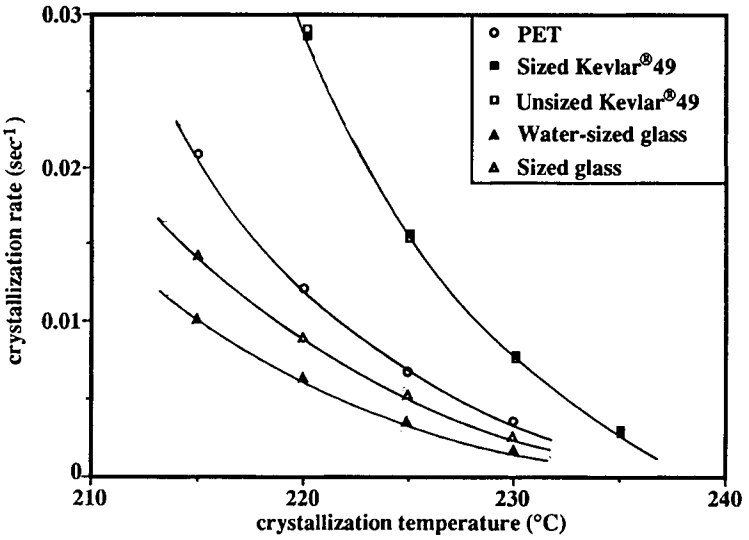

Figure 6 Crystallization rate ($1/t_{1/2}$) as a function of crystallization temperature for fiber-reinforced PET.

crystallization half-time, $t_{1/2}$, is the time at which half the area under the isothermal crystallization peak has been generated. Figure 5 shows the crystallization rate of the unreinforced PET samples as a function of crystallization temperature. Crystallization rate decreases strongly with increasing crystallization temperature, since the driving force for crystallization is the undercooling from the melt, and this is reduced at higher crystallization temperatures. At any given temperature, the rate of crystallization of nucleated PET is much greater than that of the other samples. The crystallization rate of plasticized PET is only slightly greater than that of PET. These effects reflect the fact that a crystallization rate based on $t_{1/2}$ emphasizes the early stages of crystal development, where, as Figure 4 shows, the plasticizing agent has little effect.

Crystallization rate as a function of crystallization temperature for the PET and modified-PET composites is shown in Figures 6, 7, and 8. For both PET and plasticized PET, the introduction of Kevlar fibers strongly enhances the rate of crystallization. This had been previously observed in crystallization of fiber-reinforced PET and may be attrib-

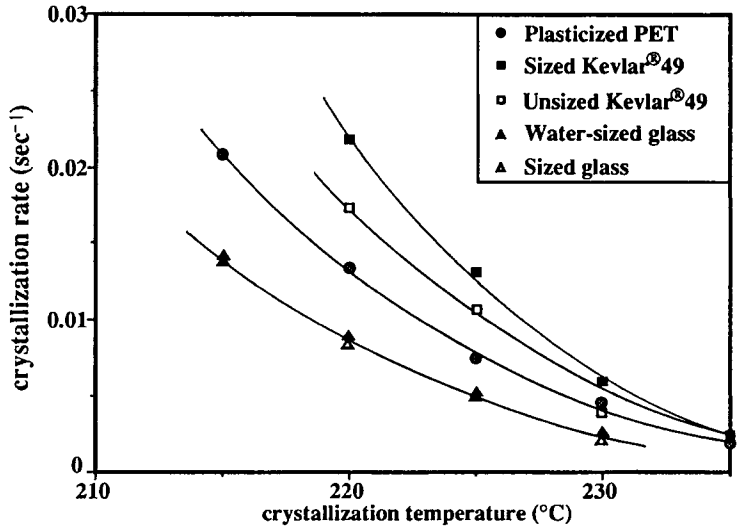

Figure 7 Crystallization rate ($1/t_{1/2}$) as a function of crystallization temperature for plasticized PET composites.

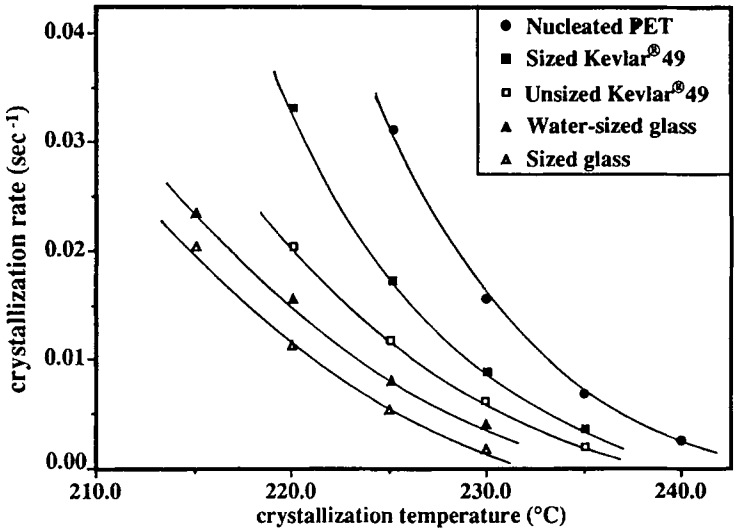

Figure 8 Crystallization rate ($1/t_{1/2}$) as a function of crystallization temperature for nucleated PET composites.

uted to a nucleating effect of the fiber surface.[24] The optical microscopy observations on model thin films, as discussed above, seem to agree with this conclusion. By providing very densely spaced sites for crystal nucleation on the fiber surface, Kevlar fibers greatly enhance the early stages of crystalline development in PET and plasticized PET. Glass fibers, in contrast, depress the crystallization rate of the PET and plasticized PET matrix polymers. This, again, can be related to the microscopy observations, where glass fibers displayed a less active nucleating ability than Kevlar. It appears that glass fibers interfere with crystal growth by providing surfaces against which growing crystals collide, thereby preventing further growth in that direction. This impingement effect appears to overwhelm any nucleating effect that glass fibers might provide, resulting in a depression of crystallization rate in glass composites.

In nucleated PET composites (Fig. 8), all fiber types depress the crystallization rate. In particular, it is interesting that Kevlar fibers, which enhance the crystallization rate in PET and plasticized PET, depress the crystallization rate in nucleated PET. The microscopy observations showed these fibers to have no ability to further nucleate the matrix. Rather, it appears that the fibers in the nucleated PET matrix act primarily as impingement points, interfering with crystal growth and resulting in a depression in crystallization rate. Furthermore, since Kevlar fibers depress the crystallization rate in the nucleated PET matrix, our conclusion that Kevlar fibers enhance the crystallization rate in the other matrices through nucleation at the fiber–polymer interface would seem to be confirmed.

Degree of Crystallinity

While the rate of crystallization of these materials is important from a processing standpoint, the degree of crystallinity of the polymer matrix is of interest as regards the final properties of the composite. The degree of crystallinity is defined as the experimental heat of crystallization divided by the heat of crystallization of 100% crystalline PET. We obtain the experimental heat of crystallization from the melting endotherm collected immediately after crystallization. The heat of fusion endotherm of the crystallized sample is used rather than the area of the crystallization exothermic peak because fusion peak areas were found to be less subject to scatter (less baseline curvature). However, it should be noted that, as a result of annealing of imperfect crystals during the fusion scan, the heat of crystallization determined from fusion data is approximately 5% higher than that determined from the exothermic peak area.

The range of values for heat of crystallization of 100% crystalline PET published in the literature is wide: from 20.0 cal/g determined by small-angle X-ray scattering[26] and using ρ_c of 1.515 g/cm^3, to 28.9 cal/g determined by diluent methods,[27] to 34.9 cal/g calculated from pressure-melting temperature methods.[28] Mehta et al. suggest that, taking into account many experiments and methods, a value of 33 $\pm$ 5 cal/g is a reasonable estimate for the heat of

Table I Degree of Crystallinity of Unreinforced PET Samples as a Function of Crystallization Temperature

	Degree of Crystallinity		
T_c (°C)	PET	Plast. PET	Nucl. PET
215	0.37 ± 0.02	0.38 ± 0.02	
220	0.36 ± 0.01	0.38 ± 0.02	
225	0.37 ± 0.01	0.38 ± 0.01	0.37 ± 0.01
230	0.38 ± 0.01	0.38 ± 0.01	0.37 ± 0.01
235		0.40 ± 0.01	0.38 ± 0.02

Note: values are mean ± standard deviation.

crystallization of 100% crystalline PET.[29] Thus, for the purposes of our degree of crystallinity calculations, we have chosen to use a value of 33 cal/g.

Table I shows final degree of crystallinity values for the unreinforced PET samples. It is interesting to note for these materials that, despite the strong influence of crystallization temperature on crystallization rate, the degree of crystallinity of all three PET samples was found to be independent of crystallization temperature. The same lack of temperature dependence was observed for the corresponding fiber composites. Therefore, results for degree of crystallinity of PET in each composite were averaged over the crystallization temperature range studied. Table II shows final degree of crystallinity values for the composite systems. Again, it is of interest to note that fiber reinforcement does not affect the ultimate degree of crystallinity achieved in these materials. This contrasts with the results obtained in our previous study of fiber-reinforced PET,[24] where fiber reinforcement produced a depression in the degree of crystallinity. It is important to note, however, that this previous study involved different PET samples from those used in the current study. For the polymer matrices in this study, it appears that, even though aramid fibers and added nucleating agent greatly enhance the rate of crystallization, the crystallites developed are ultimately no less perfect than those that grow slowly. We do note that there appears to be a small depression in the degree of crystallinity for the nucleated PET composites. However, we also note that the magnitude of possible depression in degree of crystallinity is within the uncertainty in the measurements.

Equilibrium Melting Temperature

The equilibrium melting temperature, T_m°, reflects the degree of crystalline perfection achieved in a semicrystalline polymer material. Using the fusion scans following isothermal crystallization at various temperatures, T_m° can be determined by the method of Hoffman and Weeks.[30] The melting temperature, T_m, of a sample previously crystallized at T_c is the temperature at which the maximum in the fusion peak occurs. On a plot of T_m as a function of T_c, the best-fit line to the data is extrapolated to its intersection with the line $T_m = T_c$. The temperature at this point of intersection is defined as the equilibrium melting temperature. Figure 9 shows a typical Hoffman–Weeks plot, and the equilibrium melting temperatures for the systems studied are summarized in Table III. It is interesting to note that the equilibrium melting temperature is the same for all systems studied, with the possible exception of the nucleated PET composites. As in the case of degree of crystallinity, it is possible that there is a small depression in T_m° in the nucleated PET composites. Figure 10 shows a plot of T_m° as a function of degree of crystallinity. The correlation between these two quantities is expected, as they are both measures of the crystalline perfection in the sample.

Glass Transition Temperature

The glass transition temperature, T_g, reflects the mobility of polymer chains and is therefore a useful complement to our isothermal crystallization studies (performed in a temperature range where mobility of all samples is quite high). The results for T_g, as determined from dynamic DSC scans, are shown in Table IV for the composites and neat polymers studied. It is interesting to note that sized Kevlar fibers depress T_g significantly in PET and nucleated PET, while increasing slightly the T_g of plasticized PET. This would seem to confirm our previous conclusion[24] that a component in the sizing for-

Table II Degree of Crystallinity of PET in Fiber-Reinforced Composites

	Degree of Crystallinity		
	PET	Plast. PET	Nucl. PET
Neat	0.37 ± 0.01	0.39 ± 0.01	0.37 ± 0.02
Unsized Kevlar	0.37 ± 0.01	0.36 ± 0.02	0.34 ± 0.02
Sized Kevlar	0.37 ± 0.02	0.39 ± 0.01	0.34 ± 0.01
Water-sized glass	0.38 ± 0.02	0.35 ± 0.02	0.35 ± 0.01
PET-compat. sized glass	0.41 ± 0.02	0.39 ± 0.01	0.34 ± 0.02

Note: values are mean ± standard deviation.

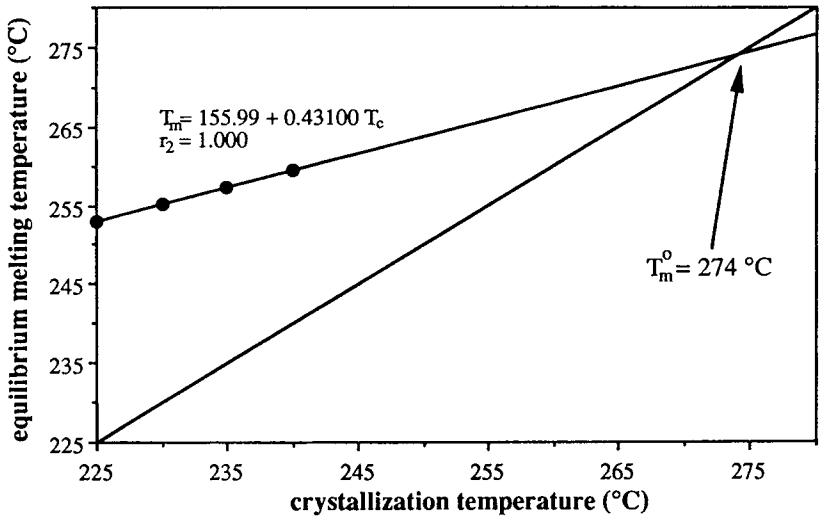

Figure 9 Hoffman–Weeks plot to determine equilibrium melting temperature of unreinforced PET.

mulation plasticizes the PET matrix. Such an effect would not be observed in a matrix that is already plasticized by an additive, in which case the sized Kevlar fibers (like the unsized) would raise T_g slightly as a result of friction or wall effects.[25] Glass fiber reinforcement, however, depresses T_g in all PET matrices, as has been previously observed.[24] This effect may be the result of chemisorbed water on glass fibers, which diffuses into the bulk polymer during composite molding, plasticizing the PET. Moisture plasticization effects have previously been reported for PET.[31,32]

Avrami Analysis of Crystallization

The kinetics of polymer crystallization can be analyzed using the Avrami model for volume fraction crystallized as a function of time

$$1 - C(t) = \exp(-Kt^n) \qquad (2)$$

where $C(t)$ is the volume fraction crystallized at time t, K is the Avrami rate constant, and n the Avrami exponent. The Avrami exponent is related to growth mechanism and geometry, while the Avrami rate constant contains nucleation and growth parameters. The model can be expressed in the well-known double logarithmic form:

$$\ln\{-\ln[1 - C(t)]\} = \ln K + n(\ln t) \qquad (3)$$

Systems obeying Avrami kinetics display linear behavior when $\ln\{-\ln[1 - C(t)]\}$ is plotted as a function of $\ln t$. All systems investigated in this study display nonlinear Avrami behavior as is shown for typical plots in Figure 11. These plots are prepared using $C(t)$ results, which are the averages of three runs for each composite sample at each crystallization temperature. Both unreinforced films and composites show two distinct linear regions. Two-step, nonlinear Avrami behavior has previously been observed for unreinforced PET (e.g., Ref. 9, 33).

This nonlinearity can be treated as two processes, each obeying Avrami behavior, occurring in series. Similar approaches have been employed in modeling the crystallization kinetics of fiber-reinforced polyphenylene sulfide[34] and polyetheretherketone.[20] Thus, K and n can be determined for the first and

Table III Equilibrium Melting Temperature (°C) as Determined by the Hoffman–Weeks Method for PET in Fiber-Reinforced Composites

	Equilibrium Melting Temperature (°C)		
	PET	Plast. PET	Nucl. PET
Neat	277 ± 3	277 ± 4	274 ± 3
Unsized Kevlar	278 ± 3	273 ± 3	267 ± 3
Sized Kevlar	276 ± 2	273 ± 3	268 ± 4
Water-sized glass	279 ± 6	274 ± 2	265 ± 3
PET-compat. sized glass	281 ± 6	275 ± 2	268 ± 2

Note: values are mean ± standard deviation.

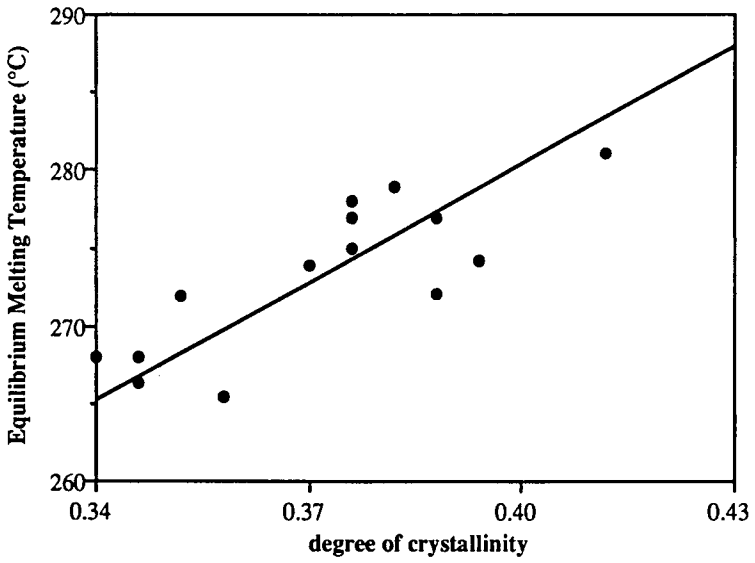

Figure 10 Equilibrium melting temperature as a function of degree of crystallinity for all systems. Degree of crystallinity results are averaged over crystallization temperature.

second processes (K_1, n_1, K_2, n_2) from the slope and intercept of the best-fit lines for each region, as seen in Figure 11. The units of K_i (i = 1 or 2) are $(\text{min})^{-n_i}$. In order to compare K_i values for crystallization having varying n_i values, the K_i values must be normalized. One normalization method involves first defining a crystallization half-time for each process from the Avrami rate constant for that process. The fraction crystallized at the beginning and end of the ith process, $C_{\text{initial},i}$ and $C_{\text{final},i}$, are determined from the Avrami plot best-fit lines and their intersection. The crystallization half-time for ith process, $t_{1/2,i}$, is then defined by using Eq. (3) and recalling that the value of $C(t)$ considered must be one-half of the total crystallinity evolved during the ith process:

$$\ln t_{1/2,i} = \frac{1}{n_i}\left\{\ln\left[-\ln\left(1 - \frac{C_{\text{final},i} - C_{\text{initial},i}}{2}\right)\right] - \ln K_i\right\} \quad (4)$$

For a given sample, the n_i values for all crystallization temperatures are then averaged to obtain $\bar{n}_i$. The normalized series Avrami rate constant, $K_{0,i}$, is calculated for each crystallization temperature using $t_{1/2,i}$ for that temperature, $\bar{n}_i$ for the temperature range, and Eq. (3):

$$\ln K_{0,i} = \ln\left[-\ln\left(1 - \frac{C_{\text{final},i} - C_{\text{initial},i}}{2}\right)\right] - \bar{n}_i(\ln t_{1/2,i}) \quad (5)$$

The units $K_{0,i}$ are $(\text{min})^{-\bar{n}_i}$, so the $K_{0,i}$'s for all crystallizations of a given composite system have the same units and can be compared.

Tables V, VI, and VII give the values for $K_{0,1}$, n_1, $K_{0,2}$, and n_2 for the PET, plasticized PET, and nucleated PET composites, respectively. Unreinforced PET, plasticized PET, and nucleated PET have n_1 values in the range of 2.5–3. The values for n_2 are much lower, ranging between 1 and 1.5 for unreinforced systems. These results are in good agreement with other studies that determined an n_1 value of 3, and an n_2 value falling between 1 and 1.5.[9,33] These values were interpreted as indicative of initial heterogeneously (athermally) nucleated spherulitic growth followed by highly constrained secondary

Table IV Glass Transition Temperature (°C) of PET in Fiber-Reinforced Composites

	Glass Transition Temperature (°C)		
	PET	Plast. PET	Nucl. PET
Neat	73.2 ± 0.2	69.7 ± 0.6	74.0 ± 1.0
Unsized Kevlar	74.3 ± 0.4	70.8 ± 2.8	74.9 ± 0.4
Sized Kevlar	65.3 ± 0.6	70.6 ± 1.0	71.0 ± 1.2
Water-sized glass	70.9 ± 3.4	66.7 ± 2.0	70.0 ± 1.0
PET-compat. sized glass	68.0 ± 3.7	66.6 ± 1.0	69.1 ± 0.6

Note: values are mean ± standard deviation.

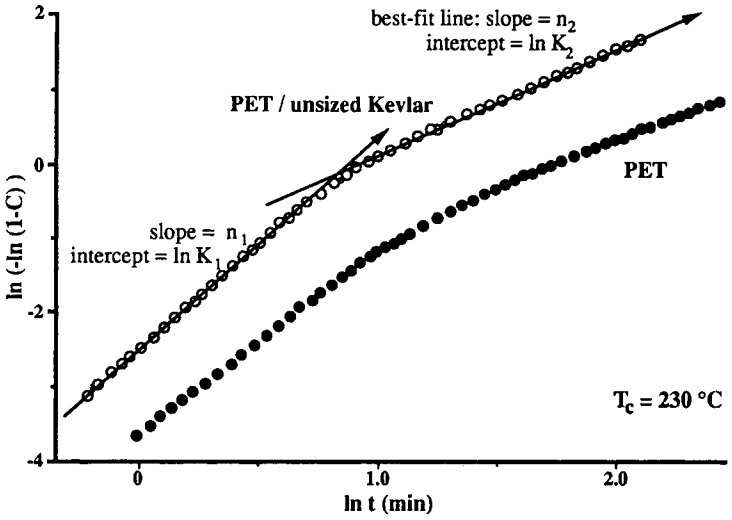

Figure 11 Typical Avrami plot for unreinforced PET and Kevlar-reinforced PET at a crystallization temperature of 230°C. Results plotted represent the average of three sets. Best-fit lines to results for Kevlar composite show series Avrami analysis approach.

crystallization.[9] These interpretations are also possible for our results. We note the possibility that the range of n_1 and n_2 values (noninteger) may be due to previous thermal history effects (multiple crystallizations), and interactions between thermal history effects and polymer additives. Alternatively, processes other than spherulitic primary crystallization followed by secondary crystallization may be

Table V Normalized Series Avrami Rate Constant, $K_{0,1}$, and $K_{0,2}$, and Series Avrami Model Exponent, n_1 and n_2, for PET Composites as a Function of Crystallization Temperature

System	T_c (°C)	$K_{0,1}$ ($\text{min}^{-\tilde{n}_1}$)	$K_{0,2}$ ($\text{min}^{-\tilde{n}_2}$)	n_1	n_2
PET	215	3.63	0.51	2.50	1.08
	220	0.93	0.28	2.54	1.38
	225	0.27	0.14	2.54	1.37
	230	0.05	0.06	2.34	1.17
Unsized	220	18.45	0.64	2.70	1.02
Kevlar	225	0.97	0.33	3.22	1.06
	230	0.09	0.16	3.13	1.22
Sized Kevlar	220	8.12	0.76	2.68	1.18
	225	0.95	0.28	2.53	1.15
	230	0.17	0.14	2.87	1.51
	235	0.02	0.04	2.28	1.32
Water-sized	215	1.05	0.27	2.04	1.37
glass	220	0.34	0.13	2.07	1.70
	225	0.15	0.06	1.98	1.31
	230	0.02	0.02	1.95	1.95
Sized glass	215	0.51	0.15	2.00	1.36
	220	0.16	0.07	2.10	1.47
	225	0.05		1.86	1.80
	230	0.02	0.01	1.75	1.22

Table VI Normalized Series Avrami Rate Constant, $K_{0,1}$, and $K_{0,2}$, and Series Avrami Model Exponent, n_1 and n_2, for Plasticized PET Composites as a Function of Crystallization Temperature

System	T_c (°C)	$K_{0,1}$ ($\text{min}^{-\tilde{n}_1}$)	$K_{0,2}$ ($\text{min}^{-\tilde{n}_2}$)	n_1	n_2
Plasticized	215	3.00	0.48	2.37	1.02
PET	220	0.62	0.24	2.35	1.05
	225	0.11	0.12	2.77	1.18
	230	0.03	0.06	2.46	1.37
Unsized	220	3.07	0.36	3.01	1.06
Kevlar	225	0.53	0.18	2.53	1.25
	230	0.02	0.04	2.57	1.29
	235	0.005	0.02	2.35	1.89
Sized Kevlar	220	6.36	0.63	2.89	1.30
	225	0.73	0.24	2.69	1.21
	230	0.07	0.08	2.66	1.19
	235	0.01	0.03	2.49	1.72
Water-sized	215	1.26	0.29	2.19	1.36
glass	220	0.39	0.14	2.10	1.57
	225	0.09	0.06	2.21	1.84
	230	0.02	0.02	2.11	1.31
Sized glass	215	1.70	0.34	1.90	1.07
	220	0.36	0.14	1.85	0.99
	225			2.03	1.32
	230	0.09	0.06	1.90	1.40

Table VII Normalized Series Avrami Rate Constant, $K_{0,1}$, and $K_{0,2}$, and Series Avrami Model Exponent, n_1 and n_2, for Nucleated PET Composites as a Function of Crystallization Temperature

System	T_c (°C)	$K_{0,1}$ ($\text{min}^{-\bar{n}_1}$)	$K_{0,2}$ ($\text{min}^{-\bar{n}_2}$)	n_1	n_2
Nucleated	225	7.71	0.62	2.88	0.76
PET	230	1.26	0.34	2.85	0.94
	235	0.13	0.17	3.11	1.17
Unsized	220	9.53	0.67	2.79	1.06
Kevlar	225	1.97	0.33	2.72	1.26
	230	0.07	0.11	2.83	0.92
	235	0.06	0.07	2.23	1.32
Sized Kevlar	220	26.28	1.14	2.80	1.17
	225	1.68	0.38	2.82	0.83
	230	0.26	0.20	2.64	1.09
	235	0.05	0.08	2.45	1.13
Water-sized	220	3.97	0.53	2.48	0.93
glass	225	0.61	0.26	2.51	1.06
	230	0.12	0.12	2.39	1.24
	235	0.05	0.06	2.42	1.19
Sized glass	220	4.15	0.49	2.69	0.83
	225	0.84	0.26	2.24	1.06
	230	0.08	0.11	2.08	1.21

occurring, resulting in variation from expected integer n values associated with these morphological interpretations.

All PET matrices reinforced by Kevlar fibers have n_1 values between 2.5 and 3, while glass fiber composites have lower n_1 values, between 2 and 2.5. These results appear to run counter to the microscopy results. Kevlar fibers induced a much more linear growth emanating from the fiber surface than did glass fibers. According to Avrami theory, linear growth results in a lower value of n than does less constrained spherical growth. Yet lower n_1 values were obtained for glass fiber composites, where optical micrographs displayed less constrained growth than for Kevlar composites. All fiber reinforced systems, like unreinforced systems, have n_2 values between 1 and 1.5. These values seem indicative of highly constrained secondary crystallization.

Tables V, VI, and VII show that the values for the Avrami rate constant for the first process, $K_{0,1}$, have a much broader range than the values for the second process, $K_{0,2}$, for all systems investigated. $K_{0,1}$ thus has a stronger temperature dependence than $K_{0,2}$. At the lower crystallization temperatures investigated, $K_{0,1}$ is much larger than $K_{0,2}$ for all systems, while at the highest crystallization temperatures (very slow crystallization) the Avrami rate constants for both processes are approximately equal. $K_{0,1}$ values for unreinforced PET and plasticized PET are similar across the temperature range studied, while $K_{0,1}$ for nucleated PET is substantially greater. $K_{0,2}$ values for all unreinforced systems are approximately equal.

For PET, plasticized PET, and nucleated PET, Kevlar fiber reinforcement resulted in an increase in $K_{0,1}$ for all crystallization temperatures investigated. Glass fiber reinforcement produced a decrease in $K_{0,1}$ for these systems. These results agree with those for the overall crystallization rate based on $t_{1/2}$. This is expected, as the overall crystallization rate emphasizes events occurring in the early stages of crystallization, as does the Avrami rate constant for the first series process, $K_{0,1}$. The effect of fiber reinforcement on the rate constant for the second process, like the effect of additives, is not as strong. These results for $K_{0,1}$ and $K_{0,2}$ agree with our previous conclusions concerning a primary crystallization process followed by constrained secondary crystallization.

From the results for $K_{0,i}$ as a function of crystallization temperature, Arrhenius plots of $\ln K_{0,i}$ as a function of undercooling from the melt, $\Delta T = T_m^\circ - T_c$, can be prepared. The activation energy of the ith crystallization process, $E_{a,i}$, is determined from the slope of the Arrhenius plot, and the frequency factor, $A_{0,i}$, from the intercept. A typical Arrhenius plot is shown in Figure 12. One can also express the overall activation energy as a combination of contributions of nucleation and growth activation energies:[34]

$$E_{a,i} = x(E_{*,i} - E_{g,i}) + \bar{n}_i E_{g,i} \qquad (6)$$

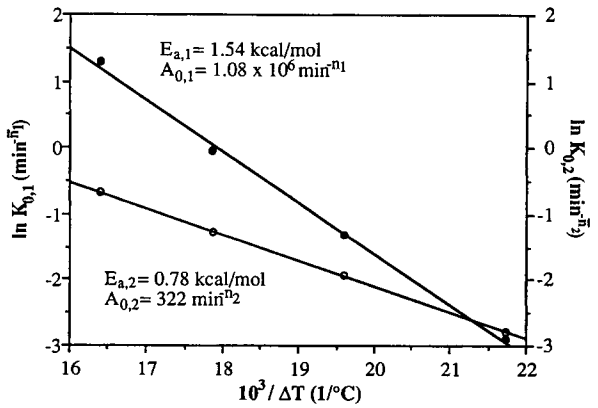

Figure 12 Plot showing Arrhenius temperature dependence of the normalized Avrami rate constant for the first and second series processes for unreinforced PET.

$$A_{0,i} = (A_{*,i})^x (A_{g,i})^{(\bar{n}_i - x)} \quad (7)$$

where x is the relative contribution of nucleation rate to $K_{0,i}$, $E_{*,i}$ the activation energy of nucleation, $E_{g,i}$ the activation energy of growth, $A_{*,i}$ the frequency factor of nucleation, and $A_{g,i}$ the frequency factor of growth. For athermally nucleated growth, there is no contribution of nucleation rate to the rate constant, so $x = 0$. The activation energy and frequency factor of growth then become

$$E_{g,i} = E_{a,i}/\bar{n}_i \quad (8)$$

$$A_{g,i} = (A_{0,i})^{1/\bar{n}_i} \quad (9)$$

The results for $E_{a,1}$, $E_{g,1}$, $A_{0,1}$, $A_{g,1}$, $E_{a,2}$, $E_{g,2}$, $A_{0,2}$, and $A_{g,2}$ are given in Table VIII.

These results show considerable variation, perhaps as a result of the relatively small range of crystallization temperatures investigated and scatter introduced in the data by thermal history effects from multiple crystallizations. However, it is clear that while the overall activation energy of the first process is larger than that of the second for all systems, the activation energy of growth is roughly the same for both processes and among all samples (within the significant scatter of the data). This result is reasonable, as the same type of chain-folded melt crystallization of PET is occurring in all cases. The overall frequency factor, $A_{0,1}$, for the first process is several orders of magnitude greater than that of the second ($A_{0,2}$). By assumption of athermal nucleation, $A_{0,i}$ is not affected by nucleation rate. However, $A_{0,i}$ presumably depends on other nucleation parameters such as density and distribution of nuclei.[34] These factors are likely to be much higher in primary than secondary crystallization. And while, for all systems, the frequency factor of growth of the first process, $A_{g,1}$, is greater than that of the second process, $A_{g,2}$, both are typically of the same order of magnitude. These results, too, seem reasonable. The development of crystallinity in the primary stage is less likely to be slowed by entanglements and other restrictions than later growth.

Modeling crystallization kinetics of PET, PET with additives, and fiber-reinforced PET using a series Avrami model with Arrhenius temperature dependence of crystallization rate gives useful insight into the nature of crystallization in these materials. There is, however, significant scatter in the results. This scatter may be indicative of complex crystallization processes, a combination of several crystal growth patterns, or thermal history effects. While the series Avrami model provides a valuable indication of the basic processes involved, a model that takes into account more complicated growth habits may be warranted.

CONCLUSIONS

In this study, we examined the effect of fiber reinforcement and polymer additives on the crystallization of PET. Plotting crystallized volume fraction

Table VIII Arrhenius Activation Energies and Frequency Factors (Overall, and for Crystal Growth) for First and Second Series Avrami Processes for All Composite Systems

Sample	$E_{a,1}$ (kcal/mol)	$E_{g,1}$ (kcal/mol)	$A_{0,1}$ ($\text{min}^{-\bar{n}_1} \times 10^{-6}$)	$A_{g,1}$ ($\text{min}^{-\bar{n}_1} \times 10^{-2}$)	$E_{a,2}$ (kcal/mol)	$E_{g,2}$ (kcal/mol)	$A_{0,2}$ ($\text{min}^{-\bar{n}_2} \times 10^{-2}$)	$A_{g,2}$ ($\text{min}^{-\bar{n}_2} \times 10^{-2}$)
PET	1.5	0.62	1.1	2.6	0.78	0.65	3.2	1.2
Unsized Kevlar	1.9	0.63	91	5.6	0.72	0.65	4.2	2.4
Sized Kevlar	1.8	0.69	72	10	0.90	0.69	24	4.0
Water-sized glass	1.2	0.60	0.02	1.4	0.97	0.65	8.7	0.9
Sized glass	1.2	0.63	0.01	1.2	1.01	0.67	6.5	0.7
Plasticized PET	1.7	0.69	4.5	4.6	0.76	0.63	2.3	0.9
Unsized Kevlar	1.9	0.74	99	12	0.93	0.66	15	1.8
Sized Kevlar	1.8	0.68	64	7.8	0.92	0.66	22	2.5
Water-sized glass	1.5	0.68	0.29	3.1	1.03	0.69	14	1.3
Sized glass	1.8	0.88	3.4	18	0.65	0.54	0.6	0.3
Nucleated PET	1.7	0.59	150	6.6	0.53	0.53	1.2	1.2
Unsized Kevlar	1.7	0.65	570	23	0.63	0.57	5.8	3.2
Sized Kevlar	1.5	0.62	60	9.1	0.55	0.53	4.0	1.2
Water-sized glass	1.6	0.60	11	5.0	0.55	0.58	3.2	0.4
Sized glass	1.4	0.59	9.3	11	0.53	0.53	1.4	1.4

as a function of time for the unreinforced films illustrated the effects of nucleant and plasticizer in the earlier and later stages of PET crystallization. Crystallization rate and T_g of PET were strongly affected by both additives and fibers. Additives were, in some cases, able to mask fiber and fiber sizing effects observed in unmodified PET, thus providing further insight into the mechanisms whereby fibers and fiber surface treatments affect polymer crystallization. Degree of crystallinity of PET was independent of crystallization temperature and the presence of additives and fibers. Kinetics of PET crystallization were analyzed using a modified Avrami model. Results indicated that two crystallization processes may occur in series, corresponding to primary crystallization and a slow secondary, or crystal perfection, process.

The authors gratefully acknowledge the assistance of Ms. Sigrid Ruetsch of TRI with the optical microscopy. Also, we thank Dr. Robert Jackson of TRI and Dr. Sue Nelsen of Hoechst Celanese for supplying the polymers used in this study, the du Pont Company for supplying the Kevlar, Dr. Pete Gaa of PPG for supplying the glass fibers, and Mr. Joe Smith of Taconic Plastics for supplying the release fabrics.

REFERENCES

1. F. van Antwerpen and D. W. van Krevelen, *J. Polym. Sci., Polym. Phys. Ed.*, **10,** 2423 (1972).
2. L. C. Sawyer and D. T. Grubb, *Polymer Microscopy,* Chapman Hall, London 1987.
3. B. P. Saville, in *Applied Polymer Microscopy,* D. A. Helmsley, Ed., Elsevier Applied Science, London, 1989, p. 125.
4. V. G. Baranov, A. V. Kenarov, and T. I. Volkov, *J. Polym. Sci., Part C,* **30,** 271 (1970).
5. S. A. Jabarin, *Polym. Eng. Sci.,* **29,** 1259 (1989).
6. S. A. Jabarin, *J. Appl. Polym. Sci.,* **34,** 85 (1987).
7. B. Günther and H. G. Zachmann, *Polymer,* **24,** 1008 (1983).
8. E. L. Lawton, *Polym. Eng. Sci.,* **25,** 348 (1985).
9. M. Patkar and S. A. Jabarin, *J. Appl. Polym. Sci.,* **47,** 1749 (1993).
10. W. P. Frank and H. G. Zachmann, *Progr. Colloid Polym. Sci.,* **62,** 88 (1977).
11. S. Fakirov, I. Seganov, and J. M. Schultz, *J. Appl. Polym. Sci.,* **32,** 3371 (1986).
12. S. Fakirov, *Polymer,* **21,** 373 (1980).
13. G. Groeninckx, H. Berghmans, and N. Overbergh, *J. Polym. Sci., Polym. Phys.,* **12,** 303 (1974).
14. S. Cheng and R. A. Shanks, *J. Appl. Polym. Sci.,* **47,** 2149 (1993).
15. S. M. Aharoni, *J. Appl. Polym. Sci.,* **29,** 853 (1984).
16. D. Garcia, *Polym. Prepr.,* **25,** 197 (1984).
17. R. Legras, C. Bailly, M. Daumerie, J. Dekoninck, and J. P. Mercier, *Polymer,* **25,** 835 (1984).
18. S. P. Kim and S. C. Kim, *Polym. Eng. Sci.,* **33,** 83 (1993).
19. G. P. Desio and L. Rebenfeld, *J. Appl. Polym. Sci.,* **44,** 1989 (1992).
20. C. N. Velisaris and J. C. Seferis, *Polym. Eng. Sci.,* **26,** 1574 (1986).
21. R. H. Burton and M. J. Folkes, in *Mechanical Properties of Reinforced Thermoplastics,* D. W. Clegg and A. A. Collyer, Eds., Elsevier Applied Science, London, 1986.
22. M. Avella, G. Della Volpe, E. Martuscelli, and M. Raimo, *Polym. Eng. Sci.,* **32,** 377 (1992).
23. C. Gauthier, J.-F. Chailan, and J. Chauchard, *Makromol. Chem.,* **193,** 1001 (1992).
24. V. Reinsch and L. Rebenfeld, *Polym. Compos.,* **13,** 353 (1992).
25. L. Rebenfeld, G. P. Desio, and J. C. Wu, *J. Appl. Polym. Sci.,* **42,** 801 (1991).
26. A. Wlochowicz and W. Przygocki, *J. Appl. Polym. Sci.,* **17,** 1197 (1973).
27. R. C. Roberts, *Polymer,* **10,** 113 (1969).
28. A. Baumgärtner, S. Blasenbrey, W. Dollhopf, E. Liska, and W. Pechhold, *Kolloid Z. Z. Polym.,* **250,** 1026 (1972).
29. A. Mehta, U. Gaur, and B. Wunderlich, *J. Polym. Sci., Polym. Phys. Ed.,* **16,** 289 (1978).
30. J. D. Hoffman and J. J. Weeks, *J. Chem. Phys.,* **37,** 1723 (1962).
31. R. Bianchi, P. Chiavacci, R. Vosa, and G. Guerra, *J. Appl. Polym. Sci.,* **43,** 1087 (1991).
32. S. A. Jabarin and E. A. Lofgren, *Polym. Eng. Sci.,* **26,** 620 (1986).
33. C. C. Lin, *Polym. Eng. Sci.,* **23,** 113 (1983).
34. G. P. Desio and L. Rebenfeld, *J. Appl. Polym. Sci.,* **45,** 2005 (1992).

Received May 25, 1993
Accepted November 17, 1993